# Calculating the Electrostatic Potential of Molecules in Solution: Method and Error Assessment

**Michael K. Gilson, Kim A. Sharp, and Barry H. Honig**

*Department of Biochemistry and Molecular Biophysics, Columbia University, 630 West 168th St., New York, New York 10032*

*Received 11 June 1987; accepted 26 August 1987*

We present a numerical method for calculating the electrostatic potential of molecules in solution, using the linearized Poisson-Boltzmann equation. The emphasis in this work is on applications to biological macromolecules. The accuracy of the method is assessed by comparisons with analytic solutions for the case of a single charge in a dielectric sphere (Tanford-Kirkwood theory), which serves as a model for a macromolecule. We find that the solutions are generally accurate to within 5%. Larger errors occur close to the charge and the dielectric boundary, but the maximum error found at ion-bonding distance (3 Å) from a charge close to the boundary (1 Å deep) is only ~15%. Several algorithmic improvements, described here, contribute to the accuracy of the method. The programs involved compose a coherent software package, called Del Phi, which goes from a Brookhaven Protein Data Bank format file to calculated electrostatic fields.

## INTRODUCTION

The electrostatic fields in and around biological macromolecules appear to be of central importance for both structure and function.[1,2] However, the modeling and calculation of these fields presents a serious challenge. Continuum electrostatic theories appear to provide a rational approach to this problem, for they incorporate the essential electrostatic features of the physical systems under study: the dielectric constants of the solvent and macromolecule, the solvent's ionic strength, and the locations and magnitudes of the charges.[3,4]

One of the major obstacles to applying continuum theories to the study of biomolecules has been the computational problem of solving the Poisson-Boltzmann equation (see e.g., Ref. 5) for systems of complicated geometry, for which analytic solutions cannot be obtained. Actually, adequate numerical techniques have long existed, but the requisite computer power has only recently become available. Orttung used the finite-element method in one of the first such applications of continuum electrostatics to molecules in solution.[6] More recently, a boundary element technique has been developed by Zauhar and Morgan.[7] The technique most commonly used for solving the Poisson-Boltzmann equation for problems in macromolecular electrostatics, however, is the finite-difference method, which was first applied to biological macromolecules by Warwicker and Watson.[8] Application of the finite-difference method to studies of Cu, Zn superoxide dismutase (SOD),[9] the Klenow fragment of DNA polymerase I,[10] and phosphglycerate mutase,[8,11] point to an important role for the electrostatic field in substrate guidance and binding. The finite-difference method has also been used in calculating redox effects in cytochrome $c_{551}$,[12] helix–helix interactions in a hypothetical spherical protein,[13] and pK changes induced by site-directed mutagenesis in subtilisin.[14,15] Many other applications of continuum electrostatic calculations in chemistry and biochemistry are possible.

However, relatively little work has been done to establish the accuracy of the numerical algorithms. Although the method of Klapper et al.[9] appears to be sufficiently accurate for the calculation of long-range potentials, such as those affecting substrate-enzyme association,[16] the grid representation of the molecule used in the finite-difference method can lead to inaccuracies in the immediate vicinity of charges and dielectric bound-

Journal of Computational Chemistry, Vol. 9, No. 4, 327–335 (1987)

CCC 0192-8651/88/040327-09$04.00

aries. For example, as previously pointed out,[11] it is difficult to obtain solutions to the Poisson-Boltzmann equation which are sufficiently accurate to be useful in calculating pK shifts of ionizable groups, when these are near other charged atoms.

We have found that it is possible to improve the accuracy substantially in the neighborhood of charges and near dielectric boundaries by modifying the algorithm of Klapper et al. to include: (1) a "focussing" technique, which makes it possible to use a finer grid; (2) a rotational averaging scheme which reduces the inaccuracies associated with representing complicated dielectric boundaries on a grid; and (3) a more spherically symmetric charge-distribution method, which increases the accuracy of short-range potentials. The present article describes these enhancements, along with several other modifications, the most important of which is the incorporation of an ion-excluding Stern layer[5] around the macromolecule. This paper then reports tests of the method's accuracy, which are based on comparisons with the case of a spherical "protein," for which analytic solutions are available in the form of the Tanford-Kirkwood theory.[3] Because intramolecular charge–charge interactions constitute the focus of the present work, and all charges belonging to a molecule lie at least one Van der Waals radius below the surface (see Methods), the accuracy is examined only for interior potentials of the "protein."

## METHODS

We employ a finite-difference method similar to that of Klapper et al.[9] The computations are carried out using a software package known as Del Phi, whose functions may be divided into: (a) preprocessing—the assignment of values to the finite-difference grid before solving the equation; and (b) actual iterative solution of the equation. The preprocessing algorithms are coded in VAX FORTRAN, and compose a program package which reads in atom coordinates in Brookhaven Protein Data Bank format, along with Van der Waals radii and a set of atomic charges, and sets up the three-dimensional ($65 \times 65 \times 65$) arrays used in the iterative solution of the Poisson-Boltzmann equation. The actual solution of the equation, which is computationally demanding, is performed by an ST-100 array processor attached to a VAX. The algorithm is coded entirely in ST-100 APL, and the multigridding algorithm of Klapper et al. is no longer used. It should be mentioned that an entirely FORTRAN version of Del Phi has also been written and is available for distribution. The major modifications that we have made to the method of Klapper et al. are as follows.

### Finite-Difference Preprocessing

Before solving the Poisson-Boltzmann equation by the finite-difference method, the values of certain physical quantities must be assigned to the grid in a way that accurately models the physical system (see Fig. 1). The points on the boundary of the grid must be assigned values for the electrostatic potential (boundary conditions); the charges in the system must be distributed onto grid points; the midpoint of each grid line connecting two

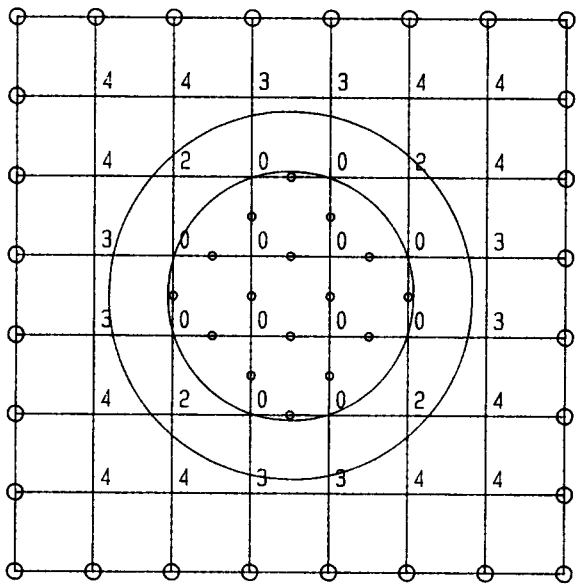


**Figure 1.** Two dimensional, $8 \times 8$ representation of electrostatic system, to illustrate preprocessing. The inner circle represents the dielectric boundary, and the outer circle represents the boundary of the Stern layer. The circled vertices at the edge must be assigned potentials to establish boundary conditions. The grid-line centers which lie inside the circular "molecule" have been assigned the interior dielectric constant, as indicated by small circles. Each nonboundary grid point has been assigned a value of $n_i$ [see eq. (1)], which here would be multiplied by $\kappa_s/4$ to obtain the Debye-Hückel parameter for each grid point. In the Stern layer around the molecule, grid-line centers have the solvent's dielectric constant but the ionic strength is below the bulk value (i.e., $n_i < 4$).

grid points must be assigned a dielectric constant—either a low interior value, or a large solvent value; and each grid point must be assigned a Debye-Hückel parameter, which is zero for the molecular interior, and is a fixed value which depends on ionic strength, around the molecule. The three-dimensional arrays containing the dielectric constant and ionic strength information are referred to as the "dielectric map" and the "ion-exclusion map," respectively. In the following, a "grid box" means one of the $64^3$ cubes making up the grid, a "grid line" is one edge of such a box, a "grid-line center" is the center of a grid line, and a "grid unit" (g.u.) is the length of a grid line.

*Focussing*

In a straightforward implementation of the finite-difference method, there is a trade-off between the accuracy of the boundary conditions (Fig. 1) and the fineness of the grid. The reason is that it is always necessary to make assumptions for the potentials at the boundary of the grid, and the assumption made—potential equals zero, for example—generally is accurate only when the edge of the grid is far from the molecule. Thus the larger the grid relative to the molecule, the more accurate the boundary conditions. On the other hand, for a fixed number of grid points, making the grid larger relative to the molecule leads to a coarser representation of the surface and of the potential map.

It is possible to retain reasonable boundary conditions while introducing a fine grid with a "focussing" technique, in which a series of finite-difference runs are performed with successively finer grids, each run having boundary conditions calculated from the potential map of its predecessor.[17] Thus, it is possible to focus into a particular region of the molecule under study in order to obtain a detailed picture of the electric fields in that region, for example in an enzyme's active site. In the present article, we describe a two-step focussing method, in which the most detailed run still contains the entire molecule, rather than a portion thereof. In the first run, the largest linear dimension of the molecule is scaled to 23% of the side length of the grid ("grid side"), and "coulombic" boundary conditions (eq. (8) of ref. 9) are used. The second run uses a grid which is finer by a factor of 4, the molecule's largest linear dimension corresponding to about 92% of the grid side. Thus the molecule fills the grid almost completely in the second run. The boundary conditions are calculated by linear interpolation from the potentials calculated in the initial coarse run. Note that new dielectric and ion-exclusion maps must be calculated for the second run.

*Distribution of Charges onto the Grid*

Rogers and Sternberg considered two methods of distributing charges onto grid points,[13] and settled on a method in which each charge is distributed over the 8 vertices of the grid box containing it, with the fraction of the charge on each vertex given by a trilinear function. The same method was used by Klapper et al.[9] However, this method leads to significant errors in the potentials near the charge when the charge is located close to the edge of the grid box. A new way of distributing charge over grid points, which produces more accurate short-range potentials, is therefore used in the present study.

Each grid point that is less than a distance $R$ from the charge location is assigned a fraction $w_i$ of the total charge given by

$$w_i = \frac{R - d_i}{\sum_i^N (R - d_i)} \tag{1}$$

where $d_i$ is the distance of the $i$th grid point from the charge, and $N$ is the total number of grid points less than $R$ away from the charge. $R$ is chosen as the smallest distance between 1.2 and 2.0 g.u. (in steps of .005 g.u.) that gives a charge distribution whose center lies within .01 g.u. of the actual charge location. If no value of $R$ satisfies this criterion, the value that gives the closest center of charge is chosen. In such cases the error in the charge location is still no more than several hundredths of a grid unit.

*Generation of the Dielectric Map*

In generating the dielectric map, every grid-line center that is contained by the solvent-accessible surface as defined by Richards[18] must be assigned the molecule's interior dielectric constant, and all other grid line centers must be assigned the dielectric

constant of the solvent (see Fig 1). (Cavities are thus assigned the solvent dielectric constant.) A 1.4 Å radius probe is normally used to represent water, and the atoms of the molecule under study are assigned standard Van der Waals radii. In some calculations, the radii are incremented by ~2.8 Å to model a layer of immobilized water at the surface. A new and faster method of generating the dielectric map (see above) has been implemented in the present version of the software package.

The first step is generation of a dot representation of a molecular surface following the older definition of Lee and Richards.[19] This surface stands one probe radius away from the molecular surface. In order to generate it, each atom is represented by a sphere of radius $r_p + r_{vdw}$, the sum of the probe radius and the atom's Van der Waals radius. The surface of each such "atom-sphere" is represented by a large number of uniformly distributed points, normally about 200 per atom. A cubing algorithm then eliminates all points which fall within any other atom sphere, leaving the desired Lee and Richards type surface. Next, the molecule is scaled to the finite-difference grid, and every grid-line center is assigned to the molecular interior if it is within an atom sphere. Finally, the Lee and Richards surface is also scaled to the grid, and a sphere of radius $r_p$ is placed at each of the surface points. Any grid-line center that falls within one of these spheres is then *reassigned* to the exterior. Thus the high dielectric solvent is considered to approach to the Van der Waals surface of each atom, unless blocked by neighboring atoms, in which case it approaches to the reentrant surface.[18]

*Generation of the Ion-Exclusion Map*

An ion-exclusion map differs from a dielectric map in that values of the Debye-Hückel parameter are assigned to actual grid points, rather than to grid-line centers (see Fig. 1). However, the first step in generating the ion-exclusion map is to generate a dielectric map, as already described, which assigns each grid-line center to the interior or exterior of the molecule. Then the Debye-Hückel parameter $\kappa_i$ assigned to grid point $i$ is given by:

$$\kappa_i = \kappa_s \frac{1}{6} n_i \qquad (2)$$

where $\kappa_s$ is the Debye-Hückel parameter for the bulk solvent, and $n_i$ is the number of grid lines (from 0 to 6) attached to grid point $i$ whose centers have been assigned to the molecular exterior. (For the 2-D case in Figure 1, where only 4 grid lines are attached to each grid point, the fraction in eq. (1) would be ¼.) Thus, grid points near the ion-exclusion region are assigned Debye-Hückel parameters between 0 and the value for bulk solvent. In order to allow for a Stern layer, the ion-exclusion map is constructed from a special dielectric map based on Van der Waals radii incremented by the desired Stern layer thickness. This dielectric map is then discarded and a new one, based on standard Van der Waals radii, is used as the dielectric map for the finite-difference calculation. This yields a region around the molecule where the dielectric constant is that of the solvent, but the Debye-Hückel parameter is zero, indicating the absence of ions. Using standard Van der Waals radii in generating the ion-exclusion map allows ions to approach to the molecular surface, and thus corresponds to a Stern layer of zero thickness.

## Solution of the Equation

*Rotational Averaging*

Even with the focussing technique, significant errors occur in the more stringent test runs. For example, for a sphere of 30 Å radius having a charge 1 Å below the surface, the errors may be as large as 50% close to the charge and the dielectric boundary. Moreover, these errors depend on the precise position and orientation of the electrostatic system relative to the grid. Although using a larger number of finite-difference grid points than the present 65 × 65 × 65 would reduce this problem, the large amount of computer memory required would be prohibitive. An alternative approach is to repeat the calculations several times with the electrostatic system rotated by different angles with respect to the grid, and then average the results. This involves generating a new grid representation of the system for each rotation angle.

In the present work, we use six rotations, with an approximately uniform distribution of $\theta$ and $\phi$ spherical angles within the first

Cartesian octant, each rotation using the two-step focussing procedure described above. In order to determine the rotationally averaged potential at a given point, the potential is obtained by linear interpolation from each rotation run,[9] and the resulting values are then averaged.

*Convergence Criteria*

The Poisson-Boltzmann equation is solved by Jacobian iteration. Since an iterative solution must be obtained for each focussing step, a full calculation using two-step focussing and averaging over six rotation angles requires 12 iterative solutions to be performed. Each iterative solution is considered to have converged when both the average and maximum changes in electrostatic potential over the entire grid are less than $10^{-6}$ kT ($6 \times 10^{-7}$ kcal/mole/$e^+$).

## ANALYSIS OF ERRORS

In order to assess the accuracy of the numerical algorithm, we compare the finite-difference results with analytic results for a unit charge in a spherical "protein" of dielectric constant $\epsilon = 2$ and a radius of 30 Å, surrounded by an infinite, homogeneous, isotropic medium of $\epsilon = 80$, containing a Debye-Hückel electrolyte at physiological ionic strength (Debye length of 8 Å). This case is solved analytically by a series[3,4,20]; we include successive terms until the next term produces a fractional change of less than $10^{-10}$. The percent error in the numerical calculations is defined as

$$\mathrm{err}(x,y,z) = 100\left|\frac{\phi_{\mathrm{num}}(x,y,z) - \phi_{\mathrm{an}}(x,y,z)}{\phi_{\mathrm{num}}(x,y,z)}\right| \quad (3)$$

where $\phi_{\mathrm{num}}$ is the numerically obtained potential, and $\phi_{\mathrm{an}}$ is the analytic result.

The error as a function of distance from the charge is explored by determining the maximum and rms error over 500 points on a sphere centered on the charge, for a sphere of increasing radius [Fig. 2(a)]. Sampling points which lie outside the low dielectric "protein" or less than 1 Å below its surface are excluded from the analysis, since in calculations on actual macromolecules all charges would lie at least 1 Å (the hydrogen atom Van der Waals radius) below the surface. The error as a function of distance from the center of the "protein" is assessed in the same way, except that

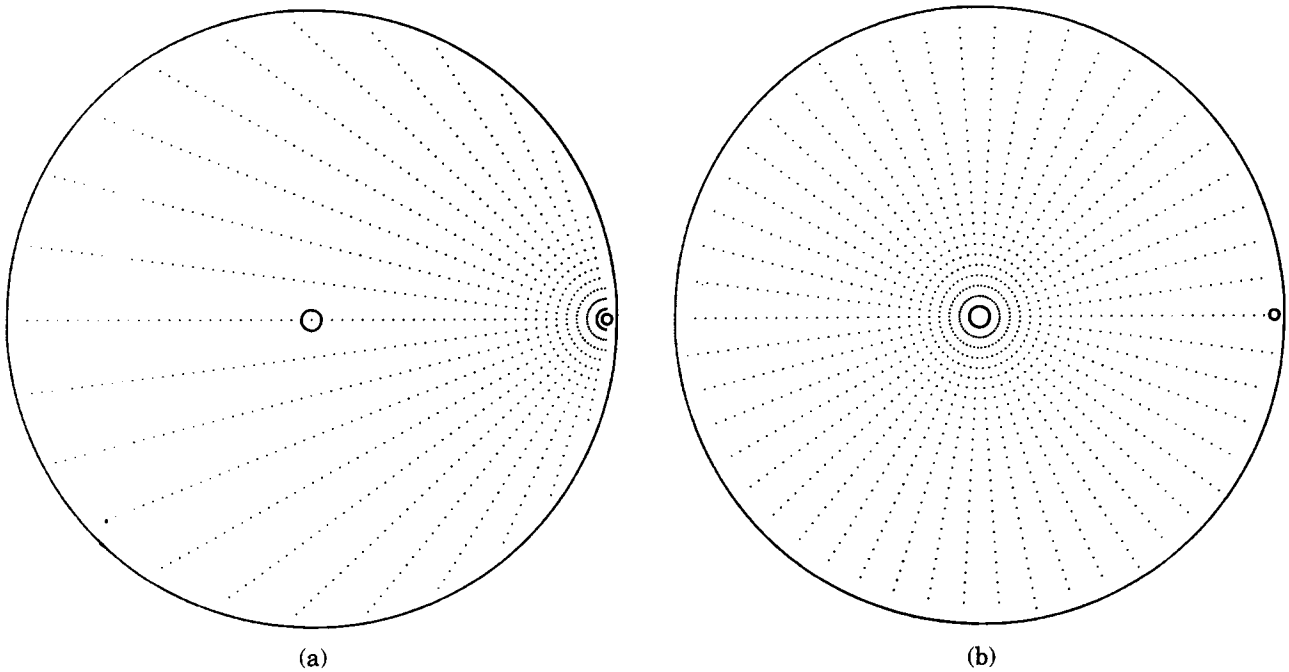


**Figure 2.** Method of obtaining errors as a function of distance from source charge (a) and center of sphere (b). A spherical "molecule" is centered on the origin (circled), and contains a source charge (small circle) 1 Å below the surface. (a) indicates concentric spheres of sampling points centered on the charge, and (b) shows concentric sampling spheres centered on the origin. Sampling points outside the sphere and in a 1 Å thick region below the surface are excluded.

the spheres of sampling points are concentric with the molecule [Fig. 2(b)].

## RESULTS

Figures 3, 4, and 5 show comparisons of numerical and analytical results for three different locations of a single charge in a low dielectric sphere of radius 30 Å, immersed in a high dielectric solvent having a Debye-Hückel type electrolyte at physiological ionic strength. In these studies, the Stern layer thickness was set at 0 Å. The Lee and Richards dot surface used in generating the dielectric and ion-exclusion maps (see Methods) contained ca. 12,000 points. For each figure, (a) gives errors as a function of distance from the charge, and (b) gives errors as a function of distance from center of the dielectric sphere (see Fig. 2(a), (b)). The upper curves show the maximum percent error (absolute value) encountered at each sampling radius, and the lower curves show the rms error for all the sampling points at each radius.

In Figure 3, the charge is located 1 Å below the surface, at $(x, y, z) = (29, 0, 0)$. As seen in Figure 3(a), the maximum errors at a given distance from the charge generally fall below 10%, though they rise to about 25% at 1 Å from the charge. The relatively large errors seen in the maximum error curve result from the fact that the sampling points lie on spheres concentric with the charge, not with the spherical "molecule," and these spheres intersect the dielectric boundary [see Fig. 2(a)]. The upper curve in Figure 3(a) is therefore a good representation of the errors 1 Å below the surface of the molecule, due to a source charge which is itself 1 Å deep. These errors are generally below 10%, but rise occasionally to near 15%. The rms errors plotted in the lower curve of Figure 3(a) show that although the errors may be as large as 25% 1 Å from the source charge, they are generally closer to about 10%. Further than about 2 Å away from the source charge, the errors are generally below 5%. These very small rms errors, averaged over all the sampling points within the sphere, imply that although errors of up to 15% may be found near the boundary, they must be quite small throughout the bulk of the molecule.

Figure 3(b) confirms this conclusion. Recall that the radii here are relative to the molecule's center, rather than relative to the source charge, as in 3(a) [see Fig. 2(b)]. It should be noted that the large errors which

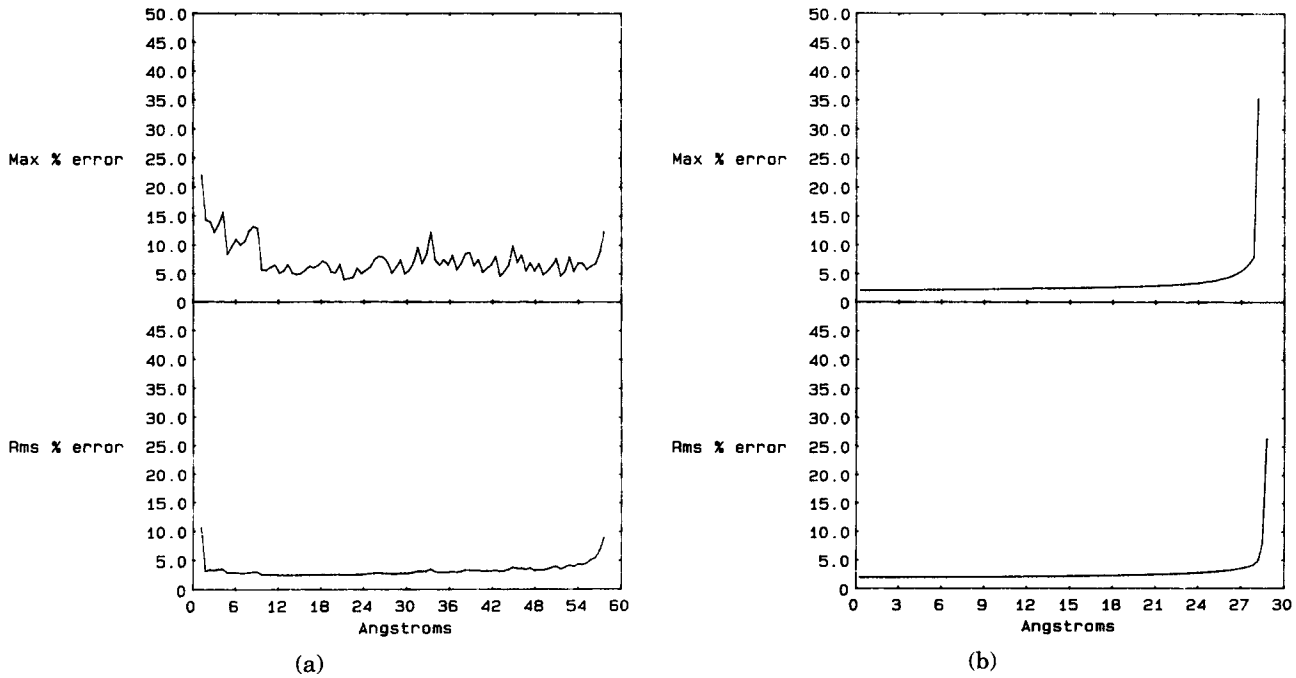


**Figure 3.** Error in numerical solution of linearized Poisson-Boltzmann equation for a charge in a low dielectric sphere, surrounded by high dielectric solvent at physiological ionic strength (Debye length = 8 Å). Sphere center at (0,0,0); charge located at (29,0,0). (a) errors as a function of distance from charge; (b) errors as a function of distance from center of sphere. In (a) and (b), upper curve is maximum percent error at given distance, lower is rms percent error.

appear at a radius of about 28 Å (Fig. 3(b), upper curve) result from the fact that the source charge is situated at 29 Å, so some sampling points are only about 1 Å away from the charge, and are thus in a region where the potential is known to be inaccurate [see Fig. 3(a)]. It should therefore be clear that the large errors at 28 Å are not those associated with the dielectric boundary 2 Å away, but to the charge 1 Å away. The errors near the boundary are well represented by the upper curve in Figure 3(a), as already noted.

Figure 4 also shows results for a charge 1 Å below the surface, but here the charge is at (12.887, 24.871, 7.506). This case is included to show the modest dependence of the accuracy on the relative orientation of the electrostatic system with respect to the finite-difference grid. The errors are a few percent larger than those for the charge at (29, 0, 0), and are similarly distributed. If the potentials were not rotationally averaged, the differences in magnitude could be substantially greater.

Figure 5 shows results for a charge 5 Å below the surface, at (25, 0, 0). Because the charge is not close to the surface, the error as a function of distance from the charge [Fig. 5(a)] becomes very small at about 2 Å, in contrast to the cases where the charge was 1 Å from the boundary, and the errors near the charge were confused with the errors associated with the boundary. The error becomes large again at about 4 Å from the charge, since some sampling points are now within an Angstrom of the surface. It is clear that the errors near this buried charge are smaller than those for a charge near the surface. However, the potential near the surface still has errors of up to 15% [top curve of Fig. 5(a)]. The lower curve of Figure 5(a) shows that the rms error throughout the sphere is extremely low for this buried charge.

Figure 5(b) shows the error in this case as a function of distance from the center of the spherical molecule. The errors are extremely low, except near the charge, which produces a peak centered at 25 Å, and near the surface. Even near the surface, however, the rms error is only about 5%. The curves in Figure 5(b) may be compared with those in Figure 3(b), in which the errors near the charge become confused with those associated with the surface. In Figure 5(b), the two sources of error produce distinct maxima. (The split in the peak near 25 Å in 5(b) results from the sparseness of the 500 sampling points on their 25 Å radius sphere.)

The severe errors near the charges represent underestimates of the analytic potentials. This seems to result primarily from the fact that the finite-difference method is less accurate when second- and higher-order spa-

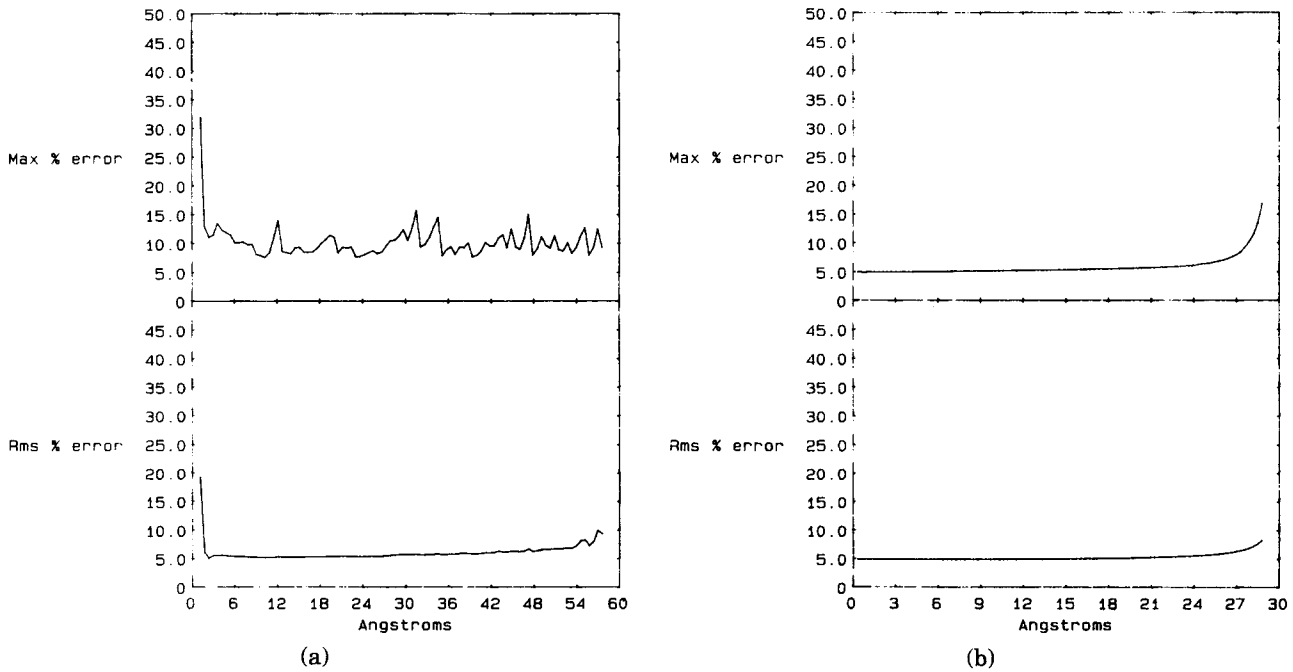


**Figure 4.** Same as Figure 1, except that charge is located at (12.887, 24.871, 7.506).

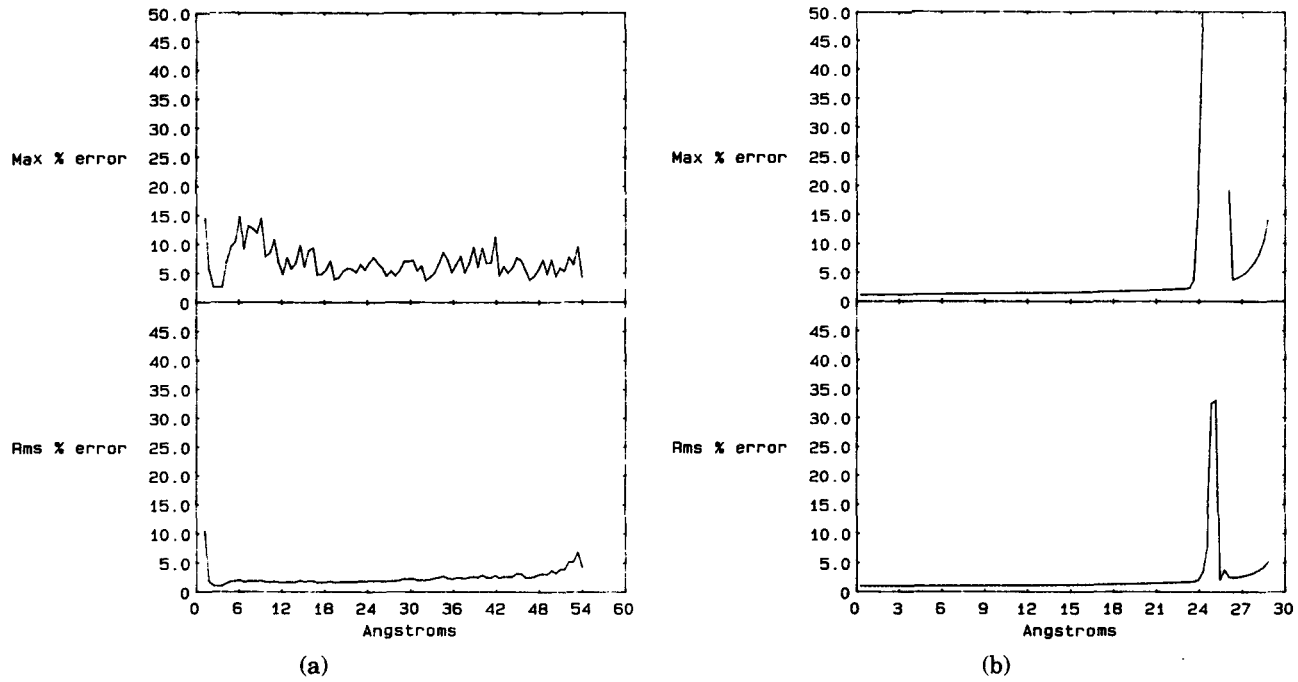


**Figure 5.** Same as Figure 1, except that charge is at (25, 0, 0).

tial derivatives of the potential are large, such as near charges. The errors near the boundary may be at least partly explained by the same limitation of the method, as higher derivatives of the potential tend to be large near boundaries as well. Another source of error near the boundary probably is the representation of a smooth surface by means of a grid. It should be emphasized, however, that the calculated potentials near the boundary lie between the correct values just inside and just outside the boundary, and thus these errors represent inaccurate "interpolations" between accurate potentials.

## DISCUSSION

This study demonstrates that it is possible and practical to obtain accurate numerical solutions of the linearized Poisson-Boltzmann equation. A range of problems in macromolecular electrostatics may now be addressed, with confidence that the results in fact represent the predictions of the theory, rather than artifacts of the numerical method. Since the worst errors arise near charges and near the dielectric boundary, it is worth noting that the maximum error found at salt-bridging distance (3 Å) away from a charge 1 Å below the surface is ~15% (Figs. 3(a) and 4(a)). If the potential is ~10 kcal/mol/$e$, the absolute error is about 1.5 kcal/mol/$e$. The rms error value at this distance is within about 5%, implying an absolute error of ca. .5 kcal/mol/$e$. It should thus be possible to obtain reasonably accurate interaction energies even for salt bridges at the molecule's surface.

The accuracy obtained here results partly from the use of rather detailed dielectric maps. In particular, the present method assigns a dielectric constant to each grid *line*[9] rather than to each grid *vertex* (see Fig. 1). Since there are three times as many grid lines as vertices, the dielectric map is actually three times more detailed than one might initially expect from the spacing of grid vertices.

The major disadvantage of using rotational averaging is that it is rather time-consuming. Fortunately, it is not always necessary. Thus, if rotating the electrostatic system relative to the grid does not affect the results significantly in initial calculations, further runs—at different ionic strengths, say—may use only one orientation.

It is perhaps surprising that the charge distribution method, which in some cases distributes charge onto grid points which lie outside the dielectric boundary, produces such accurate results. However, tests in which the charge was constrained to stay within the boundary did not improve the results, and that restriction was not incorporated.

Cases for which problems may remain are those in which charges lie very close to each other, as for a hydrogen and its hydrogen bond acceptor. The concern is that the errors can reach about 25%, and the energies involved are large, so the error may be large in absolute terms as well. These errors can probably be reduced by averaging over a larger number of rotation angles. The interaction of salt-bridge partners, which are separated by about 3 Å, will be considerably more accurate, as noted above.

We thank Hillary S. Rodman Gilson for her helpful suggestions. This work was supported by NIH grant GM-30518.

## References

1. J. B. Matthew, *Ann. Rev. Biophys. Biophys. Chem.*, **14,** 387 (1985).
2. B. Honig, W. Hubbell, and R. Flewelling, *Ann. Rev. Biophys. Biophys. Chem.*, **15,** 163 (1986).
3. C. Tanford and J. G. Kirkwood, *J. Am. Chem. Soc.*, **79,** 5333 (1957).
4. M. K. Gilson, A. Rashin, R. Fine, and B. Honig, *J. Mol. Biol.*, **183,** 503 (1985).
5. O'M. Bockris and A. K. N. Reddy, *Modern Electrochemistry,* Plenum Press, New York, 1973.
6. W. H. Orttung, *Ann. N.Y. Acad. Sci.*, **303,** 22 (1977).
7. R. J. Zauhar and R. S. Morgan, *J. Mol. Biol.*, **186,** 815 (1985).
8. J. Warwicker and H. C. Watson, *J. Mol. Biol.*, **157,** 671 (1982).
9. I. Klapper, R. Hagstrom, R. Fine, K. Sharp, and B. Honig, *Proteins,* **1,** 47 (1986).
10. J. Warwicker, D. Ollis, F. M. Richards, and T. A. Steitz, *J. Mol. Biol.*, **186,** 645 (1985).
11. J. Warwicker, *J. Theor. Biol.*, **121,** 199 (1986).
12. N. K. Rogers, G. R. Moore, and M. J. E. Sternberg, *J. Mol. Biol.*, **182,** 613 (1985).
13. N. K. Rogers and M. J. Sternberg, *J. Mol. Biol.,* **174,** 527 (1984).
14. M. K. Gilson and B. Honig, *Nature,* **330,** 84 (1987).
15. M. K. Gilson and B. Honig, *Proteins* in press.
16. K. Sharp and B. Honig, *Science,* **236,** 1460 (1987).
17. D. McAllister, J. R. Smith, and N. J. Diserens, *Computer Modeling in Electrostatics,* Research Studies Press, Wiley, New York, 1985.
18. F. M. Richards, *Ann Rev. Biophys. Bioeng.*, **6,** 151 (1977).
19. B. Lee and F. M. Richards, *J. Mol. Biol.,* **55,** 379 (1971).
20. T. L. Hill, *J. Phys. Chem.*, **60,** 253 (1956).